Yan, G. L., P. L. Biundo, and F. Li. 2026. Mechanism of calcium chloride addition in enhancing the carbothermic reduction of quartz. In *Silicon for the chemical and solar industry XVIII*, edited by M. Tangstad, H. Rong, A. Valderhaug, B. Andresen, H. Dalaker, and I. G. Page. Kristiansand, Norway, September 7–10, 2026.
https://doi.org/10.55669/oa900830

# Mechanism of calcium chloride addition in enhancing the carbothermic reduction of quartz

**G.L. Yan[1], P.L. Biundo[2], and F. Li[1,3,4*]**

[1]Department of Materials Science and Engineering, Lanzhou University of Technology, Lanzhou, P. R. China

[2]Department of Materials Science and Engineering, Norwegian University of Science and Technology, Trondheim, Norway

[3]State Key Laboratory of Advanced Processing and Recycling of Non-ferrous Metals, Lanzhou, P. R. China

[4]Gansu Provincial Engineering Research Center for Industrial Silicon, Lanzhou, P. R. China

*Contact e-mail: li.feicn@hotmail.com

*Keywords: Quartz; Calcium chloride; High-temperature melting; Carbothermic reduction; TG–DTG; Thermodynamic analysis*

**Abstract –** The carbothermic reduction of quartz is a key reaction in silicon production and is closely related to quartz softening, mass-loss behaviour of carbon-containing mixtures, and phase evolution. China is a major producer of industrial silicon, and $CaCl_2$ is sometimes added to the furnace burden in Chinese industrial silicon practice to improve furnace operation and productivity. However, its effect on quartz behaviour and carbothermic-reduction-related characteristics remains insufficiently understood. In this study, high-temperature melting experiments, TG–DTG tests, and FactSage equilibrium calculations were used to investigate the effects of $CaCl_2$ addition on high-purity quartz, the $SiO_2$–C system, and liquid- and gas-phase evolution. The results show that $CaCl_2$ markedly lowers the characteristic temperatures of quartz. As the $CaCl_2$ addition increased from 0 to 1.0 wt.%, the softening temperature ($T_S$) decreased from 1798 °C to 1745 °C, and the hemispherical temperature ($T_H$) decreased from 1836 °C to 1776 °C. TG–DTG results showed that the maximum mass-loss rate reached 2.90 % $\cdot min^{-1}$ at 0.8 wt.% $CaCl_2$, compared with 1.48 % $\cdot min^{-1}$ for the additive-free sample. Increasing the addition to 1.0 wt.% further increased the final mass loss, but reduced the maximum mass-loss rate to 2.08 % $\cdot min^{-1}$. FactSage calculations indicated that $CaCl_2$ promotes the formation of liquid salt at approximately 770–1550 °C and shifts the rapid growth of liquid slag from about 1720 °C to 1690 °C. $CaCl_2$ did not markedly change the equilibrium generation window of CO and SiO, whereas chlorine-containing gaseous species increased with addition. These results indicate that, under the present experimental conditions, 0.8 wt.% $CaCl_2$ gave the highest maximum mass-loss rate, while higher additions may contribute additional mass loss through chlorine-containing volatilization.

## 1. INTRODUCTION

Silicon is an important basic raw material for photovoltaics, silicones, semiconductors, and aluminium–silicon alloys. Its stable supply is therefore important for the development of renewable-energy and electronic-information industries. According to the U.S. Geological Survey, global silicon production in 2024 was about 4.6 million t, of which China accounted for about 3.9 million t, corresponding to approximately 84.8% of the reported global production (U.S. Geological Survey, 2025). In silicon smelting, stabilising the furnace burden, controlling the reaction state in the furnace, and improving the utilization of silicon resources are important operational objectives. According to plant-survey information obtained by the authors, $CaCl_2$ may be added in some Chinese industrial silicon operations at levels up to approximately 10–15 kg per tonne of quartz, depending on furnace condition and raw-material behaviour. The addition range of 0–1.0 wt.% used in this study corresponds to low-level $CaCl_2$ addition and covers additions up to approximately 10 kg per tonne of quartz. This range was selected to examine the effect of low $CaCl_2$ addition under controlled laboratory

conditions while avoiding excessive salt enrichment and chloride-related volatilization, which would complicate the interpretation of quartz softening, mass-loss behaviour, and gas-phase evolution.

Silicon is mainly produced through the high-temperature carbothermic reduction of quartz by carbonaceous reductants in submerged arc furnaces. This process is not a single reaction, but involves several coupled steps, including intermediate SiC formation, generation and transport of SiO gas, and further reaction between $SiO_2$ and SiC. It is therefore a typical high-temperature multiphase reaction system (Schei, Tuset, and Tveit, 1998; Ringdalen and Tangstad, 2012; Folstad et al., 2021; Sindland and Tangstad, 2021). Quartz is not only the main silicon source, but also a key raw material affecting the formation of reaction interfaces and mass-transfer conditions. During heating, quartz undergoes polymorphic transformation, volume change, cracking, softening, and melting. The high-temperature morphological evolution of different industrial quartz types can differ substantially and can further influence their behaviour under silicon-production conditions (Li, Tangstad, and Ringdalen, 2018; Metherall et al., 2023). Previous studies have shown that, in $SiO_2$–SiC systems, increasing temperature and the degree of $SiO_2$ melting are important for reaction progress, and that the transformation of quartz to cristobalite can promote SiC formation in $SiO_2$–C systems (Folstad et al., 2021; Tian et al., 2024). Studies on quartz–carbon pellets have also shown that the nature of the carbon source, particle contact state, and gas transport conditions all affect high-temperature reaction behaviour (Li and Tangstad, 2018; Li, Tangstad, and Ringdalen, 2018). Clarifying how $CaCl_2$ affects the high-temperature softening and melting behaviour of quartz and the reaction characteristics of carbon-containing systems is therefore important for understanding its role in industrial silicon production.

Additive control provides a feasible approach for improving the carbothermic reduction behaviour of $SiO_2$. It has been reported that a small amount of $K_2CO_3$ can increase the maximum mass-loss rate of silicon-related carbothermic reduction systems, indicating that additives may influence $SiO_2$ carbothermic reduction by changing the local high-temperature reaction environment (Zhou et al., 2020). However, different additives have different melting behaviours, liquid-phase formation routes, and high-temperature action paths. Therefore, results obtained for carbonate additives cannot be directly used to explain the role of $CaCl_2$. $CaCl_2$ has a relatively low melting point and can form a molten salt phase at an early stage of heating. It may therefore preferentially change the high-temperature interfacial state at the surface of $SiO_2$ particles and at local contact regions. Phase-equilibrium studies have shown that the introduction of $CaCl_2$ changes the liquid-phase formation conditions in the $SiO_2$–$CaCl_2$ binary system and the CaO–$SiO_2$–$CaCl_2$ ternary system (Wang and Morita, 2016). In addition, studies on the dissolution of calcium silicates in molten $CaCl_2$ have shown that silicate species can migrate in the molten-salt medium (Cheng and Yang, 2023). Although these results cannot be directly equated with the reaction mechanism in the $SiO_2$–C–$CaCl_2$ carbothermic reduction system, they provide useful reference for understanding how $CaCl_2$ molten salt may affect local migration of silicon-containing species and interfacial mass transfer.

Overall, previous studies have clarified the key reaction paths in silicon production, the high-temperature structural and morphological changes of quartz, the effect of additives on carbothermic reactivity, and the regulation of liquid-phase relations in $SiO_2$-containing systems by $CaCl_2$. However, the specific role of low-level $CaCl_2$ addition in the $SiO_2$–C carbothermic reduction system is still not well understood. In particular, the relationship between $CaCl_2$ addition, quartz softening and melting, overall mass loss of carbon-containing samples, and liquid-phase evolution remains insufficiently clarified.

In this study, quartz was used as the research object to examine the effect of $CaCl_2$ addition on its high-temperature behaviour and carbothermic reduction process. High-temperature in situ image acquisition was used to record the morphological changes of $SiO_2$–$CaCl_2$ samples during heating, and the initial deformation temperature ($T_D$), softening temperature ($T_S$), and hemispherical temperature ($T_H$) were determined to analyse the effect of $CaCl_2$ on quartz softening and melting. Thermogravimetric analysis (TG–DTG) was used to compare the mass-loss characteristics of the $SiO_2$–C system with different $CaCl_2$ additions. FactSage equilibrium thermodynamic calculations were further used to analyse the temperature-dependent evolution of the molten salt phase, liquid slag phase, and main gaseous species. Based on these results, the relationships among $CaCl_2$ addition, high-temperature softening and melting of quartz, mass-loss behaviour of the carbon-containing system, and liquid-phase evolution were discussed to provide experimental evidence and thermodynamic support for understanding the effect of $CaCl_2$ on quartz carbothermic reduction.

## 2. EXPERIMENTAL MATERIALS AND METHODS

### 2.1 Experimental materials

The quartz used in the experiments was crushed, ground, and sieved, and the -200 mesh (≤75 μm) powder fraction was used for sample preparation. Its chemical composition was determined by X-ray fluorescence (XRF) and is reported as oxide-equivalent mass fractions in Table I. N911 carbon black was used as the reductant, and analytical-grade anhydrous $CaCl_2$ was used as the additive.

**Table I:** Chemical composition of the quartz used in this study (wt.%)

| Compound | $SiO_2$ | $Fe_2O_3$ | $Al_2O_3$ | CaO | $TiO_2$ | Others |
|---|---|---|---|---|---|---|
| Content | 99.760 | 0.010 | 0.010 | 0.001 | 0.015 | 0.204 |

The initial morphology of the quartz powder is shown in Figure 1. After grinding and sieving, the powder particles were irregular in shape and were used for subsequent pellet preparation.

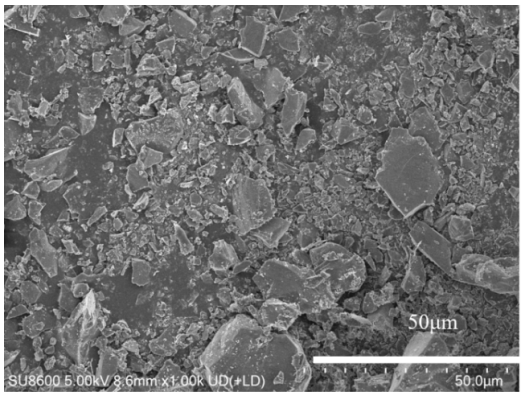


**Figure 1:** SEM morphology of the quartz powder

### 2.2 Sample preparation

Samples for the carbon-free high-temperature melting experiments and carbon-containing samples for TG–DTG tests were prepared separately according to the purpose of each test.

The samples for the high-temperature melting experiments were prepared by mixing quartz powder with $CaCl_2$. The $CaCl_2$ additions were 0, 0.1, 0.15, 0.3, 0.6, and 1.0 wt.%, all calculated on the basis of the total mass of the mixed sample. After homogeneous mixing, the powders were pressed into cylindrical specimens with a diameter of 4 mm and a height of 4 mm to

evaluate the effect of $CaCl_2$ on the high-temperature softening–melting behaviour and contour spreading of quartz.

The TG–DTG samples consisted of quartz powder, N911 carbon black, and $CaCl_2$. The quartz powder was passed through a 200-mesh sieve before sample preparation. A deliberately $SiO_2$-rich charge composition was used for the TG–DTG samples, with a molar ratio of n(C):n($SiO_2$) = 1:3. This ratio was not selected as the stoichiometric ratio for SiC formation, but was designed to retain excess $SiO_2$ after the initial formation of SiC, so that the subsequent reaction between the formed SiC and excess $SiO_2$ to generate SiO(g) and CO(g) could be considered. The $CaCl_2$ additions were 0, 0.1, 0.5, 0.8, and 1.0 wt.%. Deionized water corresponding to 8 wt.% of the powder mass was added as a temporary binder during pellet preparation. The raw materials for each group were thoroughly mixed and pressed into pellets with a mass of approximately 2.8 g to investigate the effect of $CaCl_2$ addition on the mass-loss behaviour of the carbon-containing system. Different $CaCl_2$ addition levels were used in the high-temperature melting experiments and the TG–DTG tests because the two experiments were designed for different purposes. The high-temperature melting experiments used more closely spaced low-addition levels to resolve gradual changes in quartz softening, hemispherical deformation, and apparent spreading behaviour, whereas the TG–DTG tests used representative addition levels to compare the maximum mass-loss rate and final mass loss of the $SiO_2$–C system. The 0, 0.1, and 1.0 wt.% additions were included in both experimental series as common reference levels. The sample preparation and TG–DTG testing procedure are shown in Figure 2.

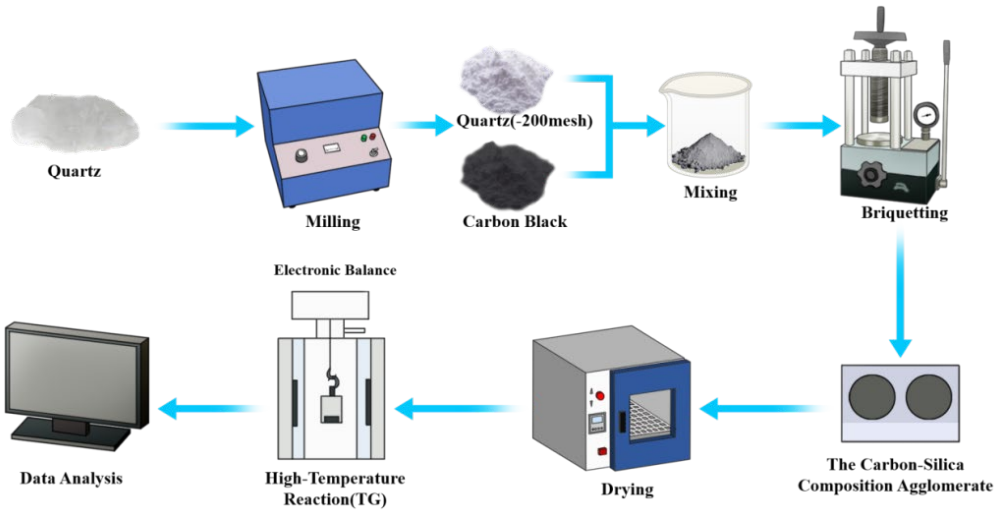


**Figure 2:** Preparation and TG–DTG testing procedure for carbon-containing samples

**Table II:** Sample compositions and experimental groups

| Experiment | Sample system | n(C):n($SiO_2$) | $CaCl_2$ addition / wt.% |
|---|---|---|---|
| High-temperature melting | $SiO_2$–$CaCl_2$ | – | 0, 0.1, 0.15, 0.3, 0.6, 1.0 |
| TG–DTG | $SiO_2$–C–$CaCl_2$ | 1:3 | 0, 0.1, 0.5, 0.8, 1.0 |

### 2.3 High-temperature melting experiment and characteristic-temperature determination

A high-temperature image-acquisition system was used to observe the morphological evolution of pressed $SiO_2$–$CaCl_2$ specimens during heating. The specimen was placed on a polished high-purity graphite substrate and heated under high-purity Ar. The heating rate was 20 °C·min$^{-1}$ from room temperature to 1600 °C and 5 °C·min$^{-1}$ above 1600 °C. The contour evolution of the specimen was continuously recorded using a monochrome industrial camera. A schematic of the setup is shown in Figure 3.

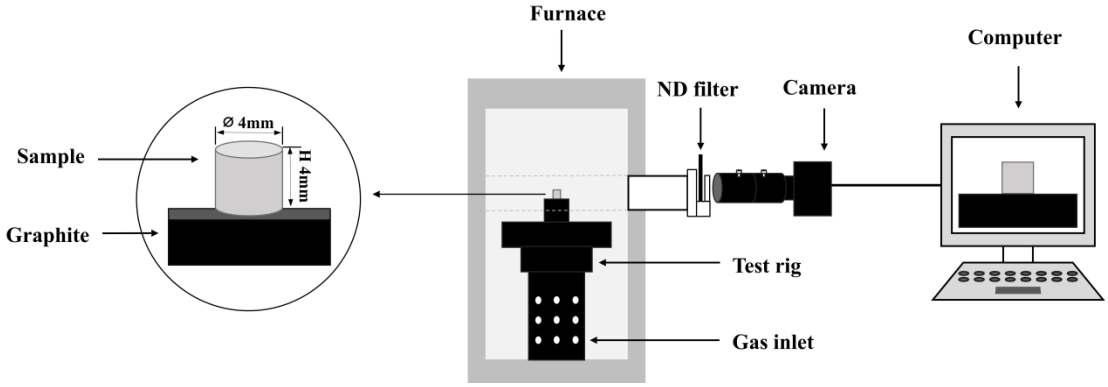


**Figure 3:** Schematic diagram of the high-temperature in situ morphological observation setup

In silicon-related studies, high-temperature in situ morphological observation has been used to evaluate the softening and melting behaviour of different industrial quartz types, and can reflect differences in the high-temperature morphological stability of quartz in the reaction temperature range (Ringdalen and Tangstad, 2016). Following this approach, the initial deformation temperature ($T_D$), softening temperature ($T_S$), and hemispherical temperature ($T_H$) were used in this study to describe the high-temperature morphological evolution of the specimens during heating. $T_D$ is defined as the temperature at which the specimen first shows identifiable contour deformation relative to the initial cylindrical morphology, and this deformation continues during subsequent heating. $T_S$ is defined as the temperature at which stable edge rounding and a clear increase in sidewall curvature first occur after initial deformation, with the specimen changing from a regular cylindrical contour towards a domed or collapsed morphology. $T_H$ is defined as the temperature at which the specimen contour first forms a hemispherical shape. The apparent contact angle between the deforming $SiO_2$–$CaCl_2$ specimen and the graphite substrate was determined from the recorded image sequences using a geometric height–base method. The graphite substrate line was used as the horizontal baseline. For each selected image, the specimen height, h, and the apparent base width in contact with the substrate, d, were obtained using image-analysis software. The apparent contact angle was then calculated according to $\theta = 2\arctan(2h/d)$. This calculation is based on a spherical-cap geometric approximation and was used to describe the macroscopic spreading behaviour of the deforming specimen. Because the specimen softened, deformed, and spread during heating, and because possible interfacial reaction with the graphite substrate cannot be excluded, the calculated value is referred to as an apparent contact angle rather than an equilibrium wetting angle. The fitted curves in Figure 6 are empirical fitting curves used only to describe the temperature-dependent trend of the apparent contact angle.

All characteristic temperatures were manually determined from continuous image sequences based on the contour evolution of each specimen, including identifiable contour deformation, edge rounding, sidewall curvature, loss of the initial cylindrical profile, and the formation of a hemispherical shape. For each $CaCl_2$ addition level, one specimen was tested; therefore, the characteristic temperatures are reported as representative values under the present experimental conditions, and no standard deviations are given. The uncertainty in the characteristic-temperature determination was estimated to be approximately ±5 °C because of the image-recording interval and manual identification of the contour transition.

### 2.4 TG–DTG test

Synchronous thermogravimetric analysis was used to investigate the effect of $CaCl_2$ addition on the mass-loss behaviour of the $SiO_2$–C system. During the test, each pellet was placed in an isostatically pressed graphite crucible and heated from room temperature to 1800 °C at a

constant heating rate of 20 °C·min$^{-1}$ under flowing Ar. The nominal Ar flow rate was set to 0.5 standard L·min$^{-1}$ using a mass-flow controller. The sample mass was recorded every 5 s. The thermogravimetric (TG) curve and its derivative (DTG) curve were calculated from the mass-change data. One TG–DTG test was performed for each $CaCl_2$ addition level; therefore, the TG–DTG parameters are reported as representative values under the present experimental conditions, and no standard deviations are given.

Previous studies have shown that quartz–carbon pellets undergo several coupled processes in silicon-related high-temperature ranges, including SiC formation, SiO generation, and gas migration. Their mass-loss behaviour is closely related to the carbon source, particle contact state, and gas-transfer conditions (Li, Tangstad, and Ringdalen, 2018; Li and Tangstad, 2018). Therefore, the maximum mass-loss rate and final mass loss were extracted from the TG–DTG curves to compare the effect of $CaCl_2$ addition on the overall mass-loss characteristics of the carbon-containing system. Because $CaCl_2$ addition may also change liquid-phase evolution and introduce high-temperature volatilization of chlorine-containing components, the mass-loss rate in the TG–DTG curves was not directly equated with the rate of a single carbothermic reduction reaction, but was used as an indicator of the overall mass-loss behaviour of the system.

### 2.5 FactSage equilibrium thermodynamic analysis

Equilibrium thermodynamic analyses for the $SiO_2$–C–$CaCl_2$ system were carried out using FactSage 8.4. FactSage is a software platform for multicomponent multiphase equilibrium calculations based on thermodynamic databases and Gibbs-free-energy minimization and has been widely used to analyse phase composition and liquid-phase evolution in high-temperature metallurgical systems (Bale et al., 2016).

The FactSage calculations were performed using a fixed input basis of 1000 g $SiO_2$ and 66.6 g C, corresponding to a molar ratio of n(C):n($SiO_2$) = 1:3. The corresponding $CaCl_2$ additions were introduced according to the selected wt.% levels. The pressure was set to 1 atm, and the atmosphere was Ar.

The masses shown in the equilibrium phase-evolution figures are calculated phase masses in grams based on this FactSage input basis, rather than mass fractions or experimentally measured masses.

The focus was on the evolution of liquid-phase composition and major gaseous species with temperature at different $CaCl_2$ additions. The databases used were FactPS, FToxid-SLAGH, and FTsalt-SALTA. FactPS was used to describe pure substances and gas species, SLAGH to describe $SiO_2$-containing oxide slag liquid, and SALTA to describe $CaCl_2$-containing salt liquid. The calculation temperature range was 600–1800 °C and was used to analyse the equilibrium evolution of liquid and gas phases at different $CaCl_2$ additions. The FactSage results represent equilibrium phase-evolution trends and are not directly equivalent to the reaction rates or mass-transfer processes occurring during actual heating.

## 3. RESULTS AND DISCUSSION

### 3.1 Effect of $CaCl_2$ addition on high-temperature morphological evolution and characteristic temperatures

During heating, all specimens evolved from a regular cylindrical contour through initial deformation and obvious softening to a molten morphology. The additive-free specimen still retained a relatively complete cylindrical contour at high temperatures, indicating the high

morphological stability of high-purity quartz. After $CaCl_2$ addition, edge rounding, sidewall bending, and top rounding occurred at lower temperatures. As the $CaCl_2$ addition increased, the development of softening and melting morphologies became more pronounced. Representative morphological changes of the specimens during heating are shown in Figure 4. The apparent specimen height in Figure 4 should be interpreted qualitatively, because the selected images were used mainly to show contour evolution rather than to compare absolute height among different specimens. At $T_D$, some specimens showed inward contraction of the sidewall and redistribution of the softened body towards the centre, which could make the apparent height remain similar to, or slightly higher than, that at 500 °C. The lower apparent height observed at $T_S$ for some samples may be related to small differences in the initial height of the pressed specimens and to macroscopic softening and collapse of the specimen contour. Therefore, $T_D$, $T_S$, and $T_H$ were determined from continuous contour evolution rather than from the absolute height in a single selected image.

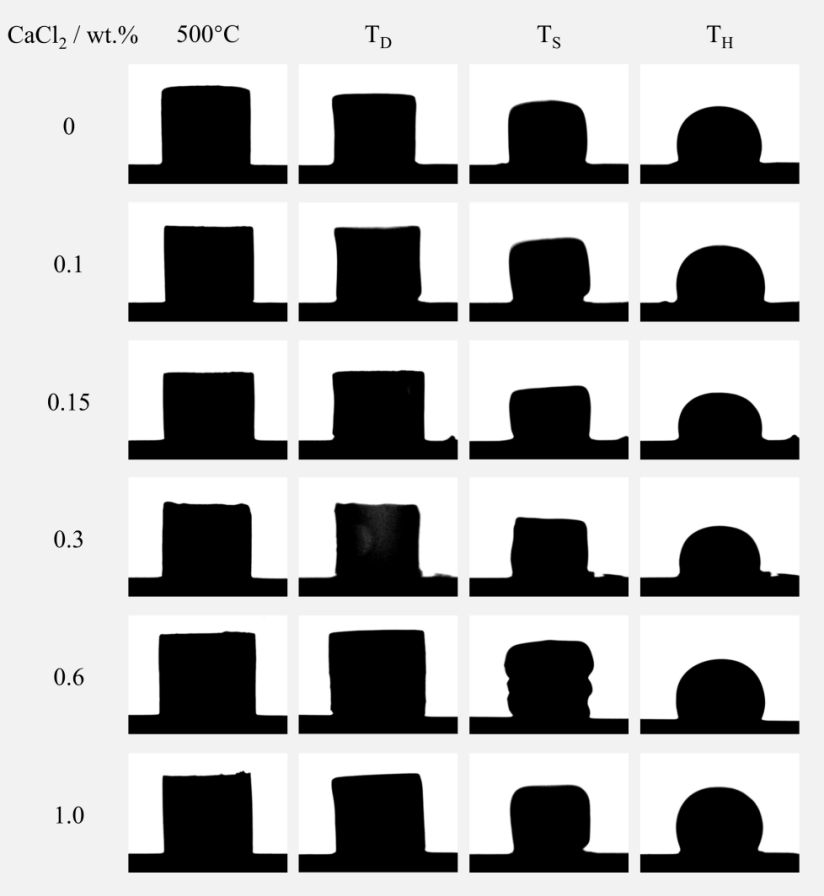


**Figure 4:** High-temperature morphological evolution of samples modified with $CaCl_2$

To quantitatively compare the effect of $CaCl_2$ on the high-temperature morphological changes of the specimens, the initial deformation temperature ($T_D$), softening temperature ($T_S$), and hemispherical temperature ($T_H$) were determined from continuous image sequences. The results are listed in Table III, and the trends are shown in Figure 5. Because one specimen was tested for each $CaCl_2$ addition level, the following discussion focuses on the overall decreasing trend rather than on small differences between neighbouring addition levels. For the additive-free sample, $T_D$, $T_S$, and $T_H$ were 1733, 1798, and 1836 °C, respectively. With increasing $CaCl_2$ addition, all three characteristic temperatures generally decreased. $T_D$ decreased from 1733 °C to about 1715–1716 °C, showing only a small change. In contrast, $T_S$ and $T_H$ decreased more markedly. At 1.0 wt.% $CaCl_2$, $T_S$ decreased from 1798 °C to 1745 °C, a decrease of 53 °C, and $T_H$ decreased from 1836 °C to 1776 °C, a decrease of 60 °C.

**Table III:** Characteristic temperatures of samples modified with $CaCl_2$

| $CaCl_2$ addition / wt.% | $T_D$ / °C | $T_S$ / °C | $T_H$ / °C |
|---|---|---|---|
| 0 | 1733 | 1798 | 1836 |
| 0.1 | 1725 | 1779 | 1825 |
| 0.15 | 1718 | 1775 | 1817 |
| 0.3 | 1717 | 1766 | 1810 |
| 0.6 | 1715 | 1752 | 1779 |
| 1.0 | 1716 | 1745 | 1776 |

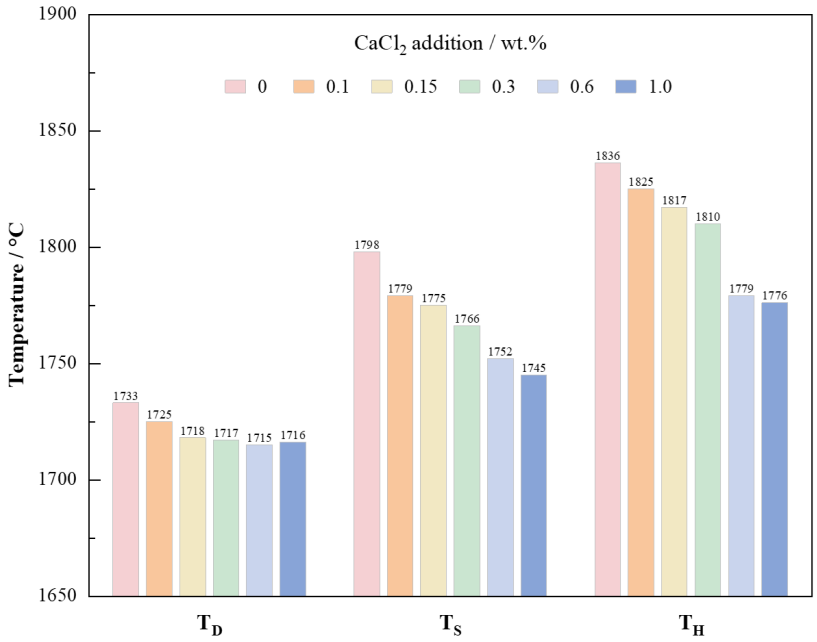


**Figure 5:** Effect of $CaCl_2$ addition on the characteristic temperatures

In summary, with increasing $CaCl_2$ addition, the initial deformation temperature changed only slightly, whereas the softening and hemispherical temperatures decreased markedly. At 1.0 wt.% $CaCl_2$, $T_S$ and $T_H$ were 53 °C and 60 °C lower than those of the additive-free specimen, respectively. It has been reported that the softening and melting temperature ranges of different industrial quartz types vary significantly, and that the high-temperature morphological state affects their contact and reaction conditions in silicon-related processes (Ringdalen and Tangstad, 2016). For $CaCl_2$-containing $SiO_2$ systems, phase-equilibrium studies further show that $CaCl_2$ addition can change the liquid-phase formation region (Wang and Morita, 2016). Therefore, the decrease in characteristic temperatures observed in this study may be related to changes in local liquid-phase evolution induced by $CaCl_2$. This relationship is further analysed using FactSage calculations in the following section.

### 3.2 Effect of $CaCl_2$ addition on apparent contact-angle evolution

The contact angle discussed in this section is the apparent contact angle between the deforming $SiO_2$–$CaCl_2$ specimen and the graphite substrate during heating. It was calculated from the specimen height and apparent base width using a spherical-cap geometric approximation. Because the specimen softened, deformed, and spread during the test, and because possible interfacial reaction with the graphite substrate cannot be excluded, the calculated angle should not be regarded as an equilibrium wetting angle. Instead, it is used as a macroscopic descriptor of the apparent spreading behaviour of the specimen on the graphite substrate. The apparent contact-angle results are therefore used for qualitative comparison of macroscopic spreading trends rather than for statistical evaluation of equilibrium wetting behaviour. As shown in

Figure 6, after $CaCl_2$ addition, the apparent contact angle decreased more noticeably at lower temperatures.

For the additive-free sample, the apparent contact angle decreased slowly with increasing temperature, from 119.5° at 1733 °C to 109.9° at 1836 °C. After $CaCl_2$ addition, the apparent contact angle decreased more markedly in the lower temperature range. The apparent contact angle of the 0.3 wt.% sample decreased from 116.4° at 1717 °C to 95.1° at 1810 °C, while that of the 0.6 wt.% sample decreased from 123.6° to 109.6° between 1765 and 1779 °C. When the addition increased to 1.0 wt.%, the apparent contact-angle change did not show a further enhancement compared with the 0.6 wt.% sample. In combination with the characteristic-temperature results, this indicates that $CaCl_2$ addition changes the softening, hemispherical deformation, and spreading behaviour of quartz at high temperature, but the effect does not increase monotonically with addition. Because $CaCl_2$ has been reported to modify liquid-phase formation in $SiO_2$-containing systems (Wang and Morita, 2016), the apparent contact-angle changes observed here may be related to local liquid formation and changes in interfacial spreading conditions induced by the additive. However, because interfacial reaction products and the spatial distribution of the liquid phase were not directly analysed in this study, the apparent contact-angle results are used mainly to characterize macroscopic spreading behaviour and are not taken as direct evidence for a specific reaction mechanism.

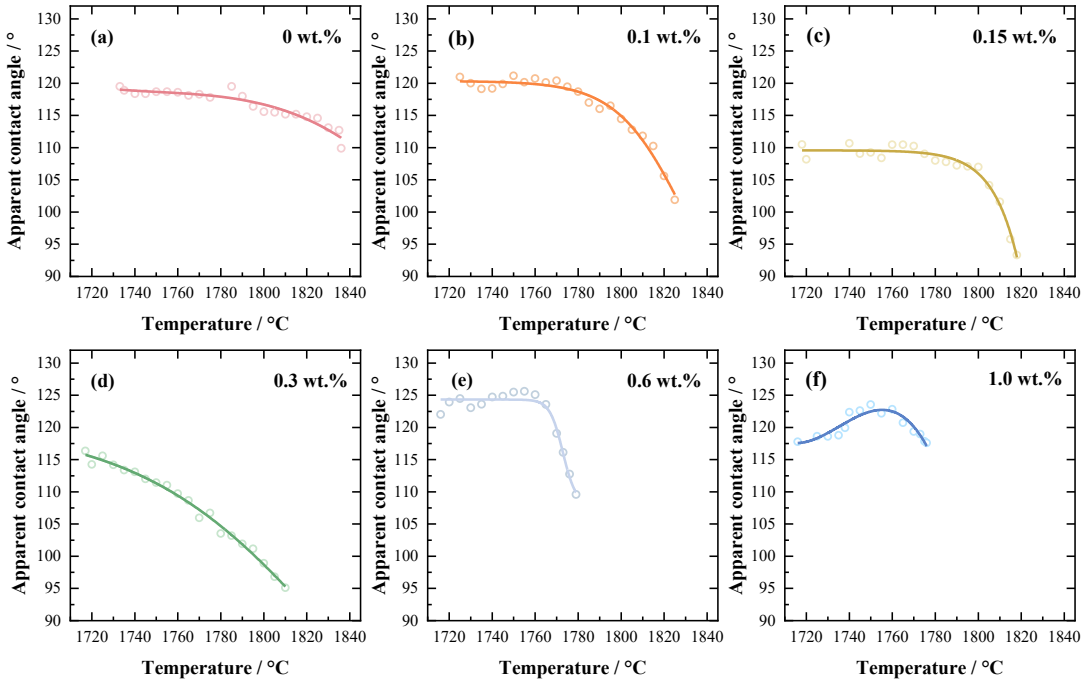


**Figure 6:** Apparent contact-angle evolution between pressed $SiO_2$–$CaCl_2$ specimens and the graphite substrate

Symbols represent measured apparent contact angles, and solid lines represent empirical fitting curves.

### 3.3 Effect of $CaCl_2$ addition on the mass-loss behaviour of the $SiO_2$–C system

The TG–DTG curves of samples with different $CaCl_2$ additions are shown in Figure 7, and the corresponding characteristic parameters are listed in Table IV. To analyse the stage-wise mass-loss behaviour reflected by the TG–DTG curves, the process was divided into Stage I and Stage II using a common boundary temperature of 1710 °C, which corresponds approximately to the transition region observed in Figure 7(b). Stage I was defined as the cumulative mass loss from the initial sample mass to 1710 °C, and Stage II was defined as the additional mass loss from 1710 °C to the end of the test. This division was used to compare the theoretical mass loss

associated with the main reaction paths with the TG-measured incremental mass loss, and does not imply that only a single reaction occurred in each stage.

Because the TG–DTG samples were prepared with a deliberately $SiO_2$-rich molar ratio of n(C):n($SiO_2$) = 1:3, carbon was the limiting reactant during the initial SiC-forming reaction. Stage I was therefore interpreted as being dominated by mass loss associated with SiC formation, as represented by Equation [1]. Stage II was interpreted as being dominated by the further reaction between the formed SiC and excess $SiO_2$, accompanied by the release of SiO(g) and CO(g), as represented by Equation [2]. These assignments are used as dominant interpreted reaction paths for theoretical comparison, rather than as proof that the actual TG process occurred through two completely separated reactions.

$$SiO_2(s,l) + 3C(s) \rightarrow SiC(s) + 2CO(g) \quad [1]$$

$$2SiO_2(s,l) + SiC(s) \rightarrow 3SiO(g) + CO(g) \quad [2]$$

The theoretical mass losses in Table V were calculated from the two-stage main reaction paths represented by Equations [1] and [2], together with the corresponding charge basis, and were used for comparison with the TG-measured stage-wise mass losses. The measured Stage I and Stage II values in Table V are incremental mass losses calculated using 1710 °C as the common boundary, and their sum corresponds to the final mass loss listed in Table IV.

For the additive-free sample, the final mass loss was 26.41%, and the maximum mass-loss rate was 1.48 % $min^{-1}$. After adding 0.1 wt.% $CaCl_2$, the final mass loss increased to 33.49%, but the maximum mass-loss rate was 1.38 % $min^{-1}$, which was not higher than that of the additive-free sample. When the $CaCl_2$ addition was further increased to 0.5 and 0.8 wt.%, the maximum mass-loss rates increased to 1.96 and 2.90 % $min^{-1}$, respectively, and the final mass losses reached 33.87% and 39.51%, respectively. The 0.8 wt.% $CaCl_2$ sample showed the highest maximum mass-loss rate, indicating that the mass-loss characteristics of the system were most pronounced at this addition.

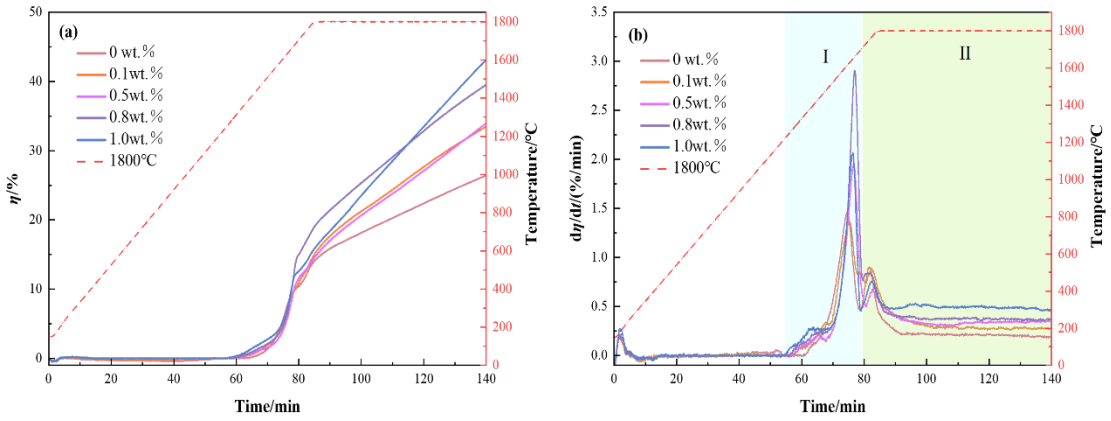


**Figure 7:** TG–DTG curves of the $CaCl_2$-modified $SiO_2$–C system

**Table IV:** TG–DTG characteristic parameters of the $CaCl_2$-modified $SiO_2$–C system

| $CaCl_2$ addition / wt.% | Maximum mass-loss rate / % $min^{-1}$ | Final mass loss / % |
|---|---|---|
| 0 | 1.48 | 26.41 |
| 0.1 | 1.38 | 33.49 |
| 0.5 | 1.96 | 33.87 |
| 0.8 | 2.90 | 39.51 |
| 1.0 | 2.08 | 42.97 |

The TG–DTG curves show that, after $CaCl_2$ addition, the mass-loss process during heating shifted overall towards lower temperature, and the corresponding DTG peak also appeared earlier. This indicates that $CaCl_2$ enabled the high-temperature mass-loss behaviour in this stage to occur at lower temperature. When the $CaCl_2$ addition was further increased to 1.0 wt.%, the final mass loss continued to increase to 42.97%, but the maximum mass-loss rate decreased to 2.08 % $\cdot min^{-1}$, lower than that of the 0.8 wt.% sample. Thus, $CaCl_2$ addition increased the overall mass loss of the $SiO_2$–C system and changed the temperature region in which mass loss occurred during heating, but its promoting effect on the maximum mass-loss rate did not increase monotonically with addition. In the present range, the 0.8 wt.% $CaCl_2$ sample had the highest concentrated mass-loss rate, whereas the 1.0 wt.% $CaCl_2$ sample had the largest cumulative final mass loss.

It should also be noted that the TG curve of the 1.0 wt.% $CaCl_2$ sample showed a different shape from those of the lower-addition samples, with a less distinct initial knee and a higher subsequent mass-loss slope. This difference may be related not only to the nominal $CaCl_2$ addition level, but also to local $CaCl_2$ distribution, mixing homogeneity, pellet structure, gas-escape pathways, and chloride-related volatilization during heating. Therefore, the higher final mass loss of the 1.0 wt.% sample is interpreted cautiously as a larger cumulative mass-loss response, rather than direct evidence of a higher carbothermic reduction degree.

Previous studies have shown that the high-temperature reduction of quartz–carbon pellets involves several coupled processes, including SiC intermediate formation, SiO generation, and gas migration, and that the carbon source and mass-transfer conditions at the particle scale can affect the overall mass-loss behaviour of the system (Li, Tangstad, and Ringdalen, 2018; Li and Tangstad, 2018). It has also been reported that $K_2CO_3$ can increase the mass-loss rate of silicon carbothermic reduction systems, indicating that additives can affect the high-temperature mass-loss characteristics of silicon-containing carbothermic systems (Zhou et al., 2020). In the $CaCl_2$-containing system investigated here, the mass change during heating may be affected not only by gas generation related to carbothermic reactions, but also by liquid-phase evolution and volatilization of chlorine-containing components. Therefore, the final mass loss and maximum mass-loss rate should be treated as characteristic parameters describing the overall mass-loss behaviour of the system, rather than being directly equated with the degree of carbothermic reduction or the rate of a single reaction.

In addition, the TG–DTG results may be affected by the properties of the pressed composite pellets, including mixing homogeneity, quartz particle-size distribution, local $CaCl_2$ distribution, pellet structure, and gas-escape pathways. Since one TG–DTG test was performed for each $CaCl_2$ addition level, the present results should be interpreted as representative trends under the present experimental conditions rather than as statistically validated differences. Therefore, the comparison among different $CaCl_2$ additions is used mainly to discuss the overall response of the system, and small differences between neighbouring additions should be interpreted with caution.

### 3.4 Thermodynamic analysis of liquid- and gas-phase evolution

FactSage was used to calculate the equilibrium liquid- and gas-phase evolution of the $SiO_2$–C–$CaCl_2$ system under Ar in order to analyse the relationship between high-temperature phase changes and the experimental mass-loss behaviour after $CaCl_2$ addition. FactSage equilibrium calculations are based on thermodynamic databases and Gibbs-free-energy minimization, and can be used to predict equilibrium phase-composition changes in high-temperature multiphase systems under specified composition, temperature, and pressure conditions (Bale et al., 2016). The calculation results reflect thermodynamic equilibrium trends rather than the

actual kinetic process during heating, which is jointly controlled by mass transfer, interfacial reactions, and volatilization. The equilibrium liquid-phase evolution at different $CaCl_2$ additions is shown in Figure 8. Enlarged views of 1670–1720 °C are included in Figures 8(b) and 8(c) to highlight the shift of the rapid liquid-phase growth region from approximately 1720 °C in the additive-free system to approximately 1690 °C in the $CaCl_2$-containing systems.

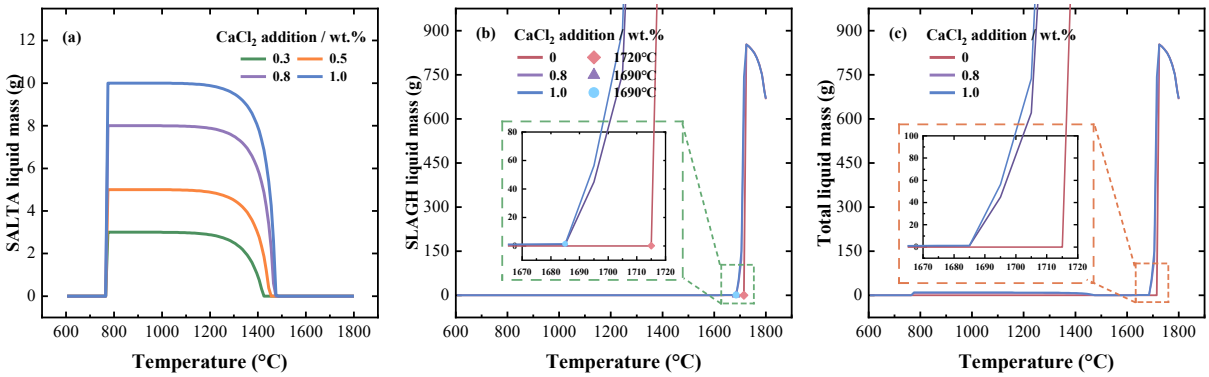


**Figure 8:** Equilibrium liquid-phase evolution in the $SiO_2$–C–$CaCl_2$ system: (a) SALTA liquid salt phase; (b) SLAGH liquid slag phase with an enlarged view of 1670–1720 °C; and (c) total liquid phase with an enlarged view of 1670–1720 °C. The y-axis represents the calculated phase mass in grams based on the FactSage input basis.

Figure 8(a) shows that the $CaCl_2$-containing systems began to form a liquid salt at about 770 °C and reached the maximum mass near 775 °C. As the $CaCl_2$ addition increased, the maximum mass of the liquid salt also increased, indicating that $CaCl_2$ first affected the liquid salt composition in the lower-temperature stage. Phase-equilibrium studies of $SiO_2$–$CaCl_2$ and CaO–$SiO_2$–$CaCl_2$ systems have shown that $CaCl_2$ addition can change the liquid-phase formation conditions in $SiO_2$-containing systems (Wang and Morita, 2016). Therefore, the low-temperature liquid salt formation trend calculated in this study is consistent with existing understanding of liquid-phase behaviour in $CaCl_2$-containing silicate systems.

With further increase in temperature, the liquid salt gradually decreased, and the high-temperature liquid-phase evolution became controlled by the liquid slag. As shown in Figure 8(b), especially in the enlarged view, the liquid slag phase in the additive-free system began to increase rapidly near 1720 °C. After $CaCl_2$ addition, the region of pronounced growth shifted to about 1690 °C. The calculation results show that $CaCl_2$ lowered by 30 °C the characteristic temperature at which a large amount of $SiO_2$ entered the liquid slag. Thus, its effect was not limited to formation of the low-temperature liquid salt, but also included an earlier growth stage of the high-temperature liquid slag.

Figure 8(c) shows that the total liquid phase in the additive-free system mainly increased rapidly after about 1720 °C with the formation of the liquid slag phase. The enlarged view further shows that $CaCl_2$ addition shifted the onset of rapid total-liquid growth to a lower temperature, close to 1690 °C, consistent with the trend observed for the liquid slag phase in Figure 8(b). In contrast, the $CaCl_2$-containing systems exhibited a two-stage evolution feature involving low-temperature liquid salt formation and earlier growth of the high-temperature liquid slag. Because the difference in total liquid mass among the systems was small at high temperature, the role of $CaCl_2$ was mainly reflected in the liquid-formation path and the temperature region of rapid liquid growth, rather than in a marked increase in the final total liquid mass. This trend is consistent with the experimental decrease in $T_S$ and $T_H$ with increasing $CaCl_2$ addition.

The experimental and calculated results are consistent in trend, although the corresponding temperature values are not identical. The high-temperature melting experiments were performed in the carbon-free $SiO_2$–$CaCl_2$ system, and $T_S$ and $T_H$ describe the macroscopic

response of the specimen when obvious softening and a nearly hemispherical morphology appear. The FactSage calculations were performed for the carbon-containing $SiO_2$–C–$CaCl_2$ system, and the characteristic temperature range reflects the pronounced growth of the liquid slag under equilibrium conditions. Formation of equilibrium species such as SiC, CO, and SiO in the carbon-containing system changes the consumption path of $SiO_2$ and the stability range of the liquid phase. In addition, minor impurities in the actual specimen, contact with the graphite substrate, and non-equilibrium spreading and mass-transfer processes may also affect the macroscopic morphological transition temperature. Therefore, the calculation results are used to explain the experimental trend and the direction of liquid-phase evolution, rather than for direct numerical correspondence with $T_S$ or $T_H$.

It has been reported that molten $CaCl_2$ can participate in the dissolution of calcium silicates and allow silicate species to migrate in the molten-salt medium (Cheng and Yang, 2023). Combined with the present calculations, the formation of low-temperature liquid salt and the forward shift of the liquid slag growth region may change the migration conditions of silicon-containing species at local interfaces. Because intermediate chlorine-containing silicate species or interfacial reaction layers were not directly identified in this study, this analysis should be regarded as a reasonable interpretation of the relationship between liquid-phase evolution and macroscopic high-temperature behaviour, rather than direct proof of specific reaction phases or mass-transfer mechanisms.

On the basis of the liquid-phase evolution analysis, the equilibrium generation of CO and SiO at different $CaCl_2$ additions was compared to further analyse the relationship between mass-loss behaviour during heating in the TG–DTG curves and gas generation related to carbothermic reduction. The results are shown in Figure 9.

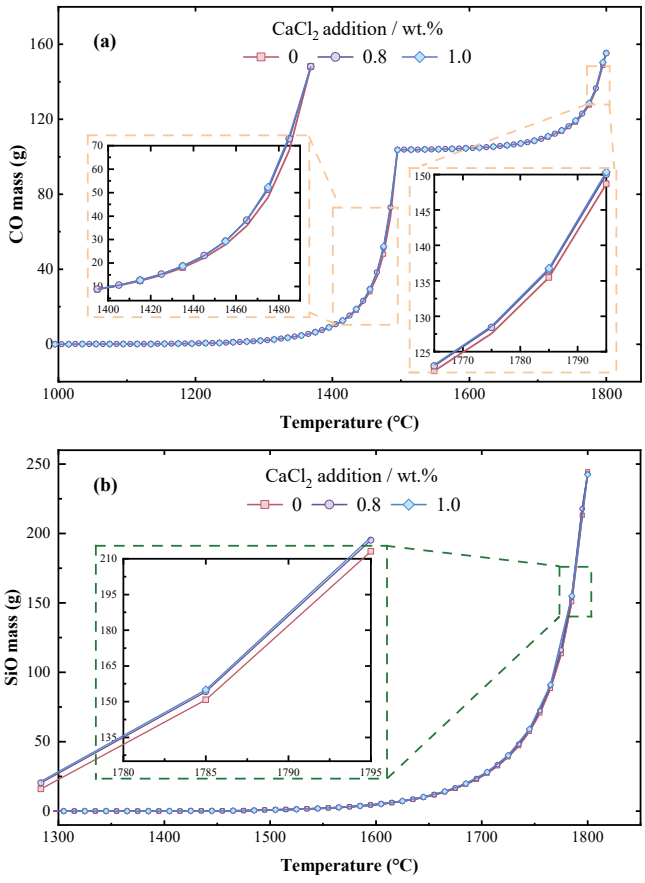


**Figure 9:** Equilibrium generation behaviour of CO and SiO: (a) CO; and (b) SiO. The insets show enlarged views

Figures 9(a) and 9(b) show that the overall calculated evolution curves of CO and SiO were similar among the different systems, indicating that $CaCl_2$ addition did not markedly change the overall equilibrium generation window of the two major gaseous species. Figure 9(a) shows that the equilibrium CO amount increased in stages with temperature. Enlarged views of the temperature region corresponding to the mass-loss process during heating in the TG–DTG curves show that the equilibrium CO amount in the $CaCl_2$-containing systems was slightly higher than that in the additive-free system. This indicates that $CaCl_2$ may increase the equilibrium tendency for CO-related gas generation in this temperature region. This change is related to the shift of the mass-loss process to lower temperature in the thermogravimetric experiment. However, because the initial equilibrium generation region of CO did not change significantly with $CaCl_2$ addition, the earlier appearance of the mass-loss process in TG–DTG cannot be simply attributed to a decrease in the thermodynamic generation onset of CO. Figure 9(b) shows that SiO increased rapidly mainly in the higher-temperature region. The enlarged view shows that the equilibrium SiO amount in the $CaCl_2$-containing systems was slightly higher than that in the additive-free system during the high-temperature rapid-growth stage, but the differences among the addition levels were small. This result suggests that $CaCl_2$ may have some effect on the SiO generation tendency in the later high-temperature stage, but this effect alone is insufficient to explain all changes in the concentrated mass-loss behaviour observed by TG–DTG.

Combining the TG–DTG experiment with gas-phase equilibrium calculations, the mass-loss process during heating occurred earlier after $CaCl_2$ addition, whereas the initial equilibrium generation regions of CO and SiO did not change markedly. This indicates that the earlier experimental mass loss was not caused by a direct decrease in the thermodynamic generation onset of the relevant gaseous products, but was more likely related to liquid-phase evolution induced by $CaCl_2$. Together with the formation of liquid salt and the shift of the liquid slag growth region shown in Figure 8, $CaCl_2$ may improve interfacial contact and apparent spreading conditions in the actual sample, thereby facilitating local mass transfer and allowing mass loss associated with CO and SiO generation to occur at lower temperature.

Compared with the small differences observed in the CO and SiO curves, the chlorine-containing gaseous species showed a more pronounced response to $CaCl_2$ addition. Their equilibrium evolution is shown in Figure 10.

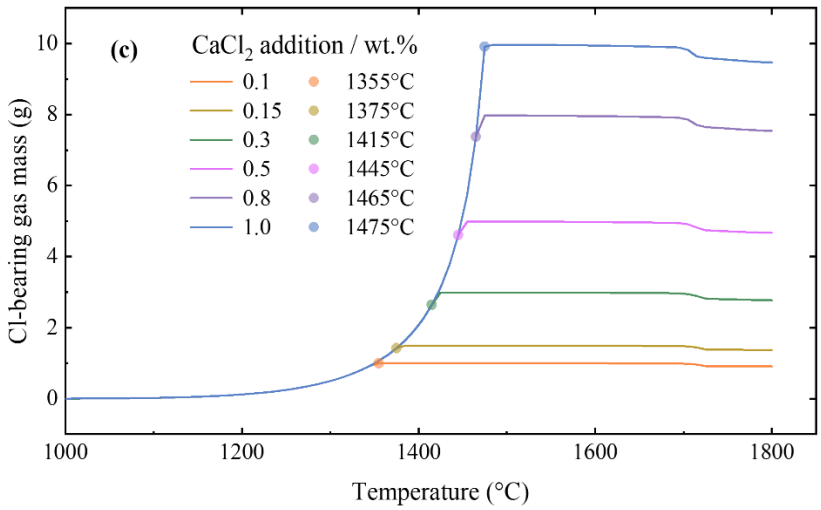


**Figure 10:** Equilibrium evolution of the total mass of chlorine-containing gaseous species

The chlorine-containing gas mainly formed rapidly in the range of 1355–1475 °C. The 0.8 and 1.0 wt.% $CaCl_2$ systems both reached their maximum values near 1485 °C, with maximum

masses of 7.98 and 9.97 g, corresponding to approximately 0.595% and 0.742% of the total system mass, respectively. This indicates that, with increasing $CaCl_2$ addition, the tendency of chlorine-containing components to volatilize into the gas phase during heating became stronger. To further compare the difference between the theoretical mass loss from the main carbothermic reactions and the experimental stage-wise mass loss, the results are listed in Table V.

**Table V:** Comparison between stage-wise theoretical mass loss and TG-measured mass loss

| $CaCl_2$ addition / wt.% | Stage I theoretical mass loss / % | Stage I measured mass loss / % | Stage II theoretical mass loss / % | Stage II measured mass loss / % |
|---|---|---|---|---|
| 0 | 9.71 | 9.95 | 27.79 | 16.46 |
| 0.1 | 9.70 | 11.54 | 27.76 | 21.95 |
| 0.5 | 9.66 | 12.05 | 27.65 | 21.82 |
| 0.8 | 9.64 | 14.76 | 27.57 | 24.75 |
| 1.0 | 9.62 | 12.17 | 27.51 | 30.80 |

Based on the stage-wise mass-loss regions defined in Figure 7 and the main reaction paths represented by Equations [1] and [2], Table V compares the stage-wise theoretical mass losses and TG-measured mass losses at different $CaCl_2$ additions. The theoretical values consider only the mass loss caused by the main $SiO_2$–C reaction paths and do not include $CaCl_2$ volatilization or the formation of other chlorine-containing gaseous species.

In Stage I, the measured mass loss of the 0.8 wt.% $CaCl_2$ sample was 14.76%, higher than 12.17% for the 1.0 wt.% sample. This agrees with the highest maximum mass-loss rate observed for the 0.8 wt.% sample in the TG–DTG curves, indicating that an appropriate $CaCl_2$ addition is more favourable for the concentrated mass-loss process during heating.

In Stage II, the measured mass loss of the 1.0 wt.% $CaCl_2$ sample reached 30.80%, higher than its theoretical value of 27.51%. In combination with Table IV, the final measured mass losses of the 0.8 and 1.0 wt.% samples were higher than the two-stage total theoretical mass losses by 2.30 and 5.84 percentage points, respectively, with the larger deviation occurring for the 1.0 wt.% sample. This trend is consistent with the increase in chlorine-containing gas mass with $CaCl_2$ addition in Figure 10, indicating that the final mass loss of high-addition samples may include not only gas release related to the $SiO_2$–C reactions, but also additional mass loss caused by volatilization of chlorine-containing components.

However, the part of the experimental mass loss exceeding the theoretical mass loss cannot be fully attributed to chlorine-containing gas. The FactSage results reflect the gas composition trend under equilibrium conditions, whereas the TG test records cumulative mass loss during actual heating and holding. The experimental mass loss is also affected by liquid formation, interfacial contact, gas escape, and non-equilibrium mass transfer. Therefore, the higher final mass loss of the 1.0 wt.% $CaCl_2$ sample indicates only a larger cumulative mass loss and does not demonstrate a higher degree of carbothermic reduction than that of the 0.8 wt.% sample.

In summary, the effect of $CaCl_2$ on the mass-loss behaviour of the $SiO_2$–C system is not controlled by a single factor. The formation of low-temperature liquid salt and the forward shift of the high-temperature liquid slag growth region may improve interparticle contact and local mass-transfer conditions, thereby allowing the concentrated mass-loss behaviour during heating to occur earlier and become enhanced. At the same time, the mass of chlorine-containing gas increased with $CaCl_2$ addition, indicating that the increase in cumulative mass loss in high-addition samples may include additive-related volatilization. Thus, 0.8 wt.% $CaCl_2$ was more favourable for increasing the concentrated mass-loss rate, whereas the higher final mass loss of the 1.0 wt.% sample cannot be interpreted directly as a further increase in

carbothermic reduction degree. The detailed mechanism responsible for the weakened rate gain at higher addition still requires further verification based on post-reaction phase analysis, interfacial microstructure, and analysis of evolved or condensed products.

## 4. CONCLUSIONS

This study investigated the effect of $CaCl_2$ addition on the high-temperature softening and melting behaviour of high-purity quartz, the mass-loss characteristics of the $SiO_2$–C system, and equilibrium liquid- and gas-phase evolution. The main conclusions are as follows:

(1) $CaCl_2$ effectively lowered the characteristic high-temperature softening and melting temperatures of quartz. As the $CaCl_2$ addition increased from 0 to 1.0 wt.%, the softening temperature $T_S$ decreased from 1798 °C to 1745 °C, and the hemispherical temperature $T_H$ decreased from 1836 °C to 1776 °C, corresponding to decreases of 53 °C and 60 °C, respectively. This indicates that $CaCl_2$ markedly changed the high-temperature morphological evolution of quartz.

(2) $CaCl_2$ addition changed the mass-loss behaviour of the $SiO_2$–C system. Within the present range, the 0.8 wt.% $CaCl_2$ sample reached a maximum mass-loss rate of 2.90 % $\cdot min^{-1}$, markedly higher than 1.48 % $\cdot min^{-1}$ for the additive-free sample. When the addition increased to 1.0 wt.%, the final mass loss further increased to 42.97%, but the maximum mass-loss rate decreased to 2.08 % $\cdot min^{-1}$. This shows that $CaCl_2$ can increase the cumulative mass loss of the system, but its promoting effect on the mass-loss rate does not continuously increase with addition.

(3) FactSage equilibrium calculations showed that $CaCl_2$ changed the liquid-phase evolution path. In the $CaCl_2$-containing system, the liquid salt mainly existed at approximately 770–1550 °C. At high temperature, $CaCl_2$ lowered the characteristic temperature at which a large amount of $SiO_2$ entered the liquid slag from 1720 °C in the additive-free system to 1690 °C. This liquid-phase evolution trend corresponds to the decrease in $T_S$ and $T_H$ observed experimentally, indicating that changes in the liquid-formation path may be an important thermodynamic factor for earlier softening and melting of quartz.

(4) Gas-phase equilibrium calculations showed that $CaCl_2$ addition did not markedly change the overall equilibrium generation windows of CO and SiO. However, the equilibrium amounts of CO and SiO in the $CaCl_2$-containing systems were slightly higher in some stage-specific growth regions. In contrast, the total mass of chlorine-containing gaseous species increased markedly with $CaCl_2$ addition. Combined with the comparison between stage-wise theoretical mass loss and TG-measured mass loss, the increase in cumulative mass loss in high-addition samples may include not only gas release related to $SiO_2$–C reactions, but also additive-related volatilization. Therefore, the higher final mass loss of the 1.0 wt.% $CaCl_2$ sample does not directly indicate a higher degree of carbothermic reduction than that of the 0.8 wt.% sample.

From an industrial perspective, the present results indicate that low-level $CaCl_2$ addition can modify the softening behaviour of quartz and the mass-loss behaviour of $SiO_2$–C mixtures under silicon-production-related conditions. The non-monotonic response of the maximum mass-loss rate suggests that increasing $CaCl_2$ addition does not necessarily lead to continuous improvement. Excessive addition may increase chloride-related volatilization and should therefore be controlled carefully. Thus, $CaCl_2$ may be considered as a low-level process-adjusting additive, but its application should consider raw-material variability, burden permeability, gas escape, and possible chlorine-containing emissions.

Overall, within the present experimental range, 0.8 wt.% $CaCl_2$ gave the highest maximum mass-loss rate in the $SiO_2$–C system. The role of $CaCl_2$ is associated with its induction of liquid salt formation, promotion of high-temperature slag-liquid evolution, and influence on high-temperature gas release behaviour. The detailed mechanism behind the weakened rate gain at higher addition still requires further verification through post-reaction phase analysis, interfacial microstructure characterization, and quantitative analysis of volatile components.

## 5. REFERENCES


Bale C.W., Bélisle E., Chartrand P., Decterov S.A., Eriksson G., Gheribi A.E., Hack K., Jung I.-H., Kang Y.-B., Melançon J., Pelton A.D., Petersen S., Robelin C., Sangster J., Spencer P., and Van Ende M.-A. 2016. FactSage thermochemical software and databases, 2010–2016. *Calphad*, Vol.54, pp.35–53.

Cheng X. and Yang X. 2023. Dissolution of calcium silicates in molten $CaCl_2$. *Metallurgical and Materials Transactions B*, Vol.54, pp.192–202.

Folstad M.B., Ringdalen E., Tveit H., and Tangstad M. 2021. Effect of different $SiO_2$ polymorphs on the reaction between SiO2 and SiC in Si production. Metallurgical and Materials Transactions B, Vol.52, pp.792–803.

Li F. and Tangstad M. 2018. Kinetic modeling of the reaction rate for quartz and carbon black pellet. Metallurgical and Materials Transactions B, Vol.49, pp.1101–1108.

Li F., Tangstad M., and Ringdalen E. 2018. Carbothermal reduction of quartz and carbon pellets at elevated temperatures. *Metallurgical and Materials Transactions B*, Vol.49, pp.1078–1088.

Metherall B., Breward C.J.W., Please C.P., and Lacey A.A. 2023. Modelling the reduction of quartz in a quartz–carbon pellet. *Journal of Engineering Mathematics*, Vol.141, Article 4.

Ringdalen E. 2015. Changes in quartz during heating and the possible effects on Si production. *JOM*, Vol.67, pp.484–492.

Ringdalen E. and Tangstad M. 2012. Reaction mechanisms in carbothermic production of silicon: Study of selected reactions. In: International Smelting Technology Symposium. Hoboken: John Wiley & Sons, pp.195–204.

Ringdalen E. and Tangstad M. 2016. Softening and melting of SiO2, an important parameter for reactions with quartz in Si production. In: Reddy R.G., Chaubal P., Pistorius P.C., and Pal U., eds. *Advances in Molten Slags, Fluxes, and Salts: Proceedings of the 10th International Conference on Molten Slags, Fluxes and Salts 2016.* Cham: Springer, pp.43–51.
https://doi.org/10.1007/978-3-319-48769-4_4

Schei A., Tuset J.K., and Tveit H. 1998. Production of High Silicon Alloys. Trondheim: Tapir Forlag.

Sindland C. and Tangstad M. 2021. Production rate of SiO gas from industrial quartz and silicon. Metallurgical and Materials Transactions B, Vol.52, pp.1755–1771.

Tian J., Wei K., Deng X., Liu Y., and Ma W. 2024. A study of the effect of quartz-to-cristobalite transformation on SiC generation in metallurgical-grade silicon production. Silicon, Vol.16, pp.3155–3164.

U.S. Geological Survey. 2025. *Mineral Commodity Summaries 2025: Silicon.* Reston, VA: U.S. Geological Survey, pp.160–161.
https://pubs.usgs.gov/periodicals/mcs2025/mcs2025-silicon.pdf

Wang Y. and Morita K. 2016. Measurement of the phase diagram of the $SiO_2$–$CaCl_2$ system and liquid area study of the $SiO_2$–CaO–$CaCl_2$ system. *Metallurgical and Materials Transactions B*, Vol.47, pp.1542–1547.

Zhou S., Chen Z., Ma W., Li S., and Zhao Y. 2020. Effect of $K_2CO_3$ as an additive agent on the carbothermic reduction process of silicon production. *Silicon*, Vol.12, pp.1575–1584.


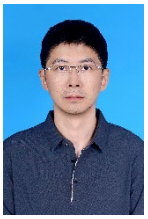


**Fei Li**

*Associate Professor, Lanzhou University of Technology*


Received a Ph.D. degree from the Norwegian University of Science and Technology in 2017. The main research interests include industrial silicon and silicon-based ferroalloy smelting, silicon functional materials, and solid waste recycling. Current work focuses on reaction mechanisms, process optimization, and sustainable utilization of silicon resources and industrial solid wastes.